The cosmic ray positron to electron ratio in the energy range 0.85 to 14 GeV

G. Barbiellini[12], G. Basini[4], R. Bellotti[1], M. Bocciolini[3], M. Boezio[12], F. Massimo Brancaccio[3], U. Bravar[12], F. Cafagna[1], M. Candusso[8], P. Carlson[10], M. Casolino[8], M. Castellano[1], M. Circella[1], A. Codino[7], G. De Cataldo[1], C. De Marzo[1], M.P. De Pascale[8], N. Finetti[7], T. Francke[10], N. Giglietto[1], R.L. Golden[6], C. Grimani[7], M. Hof[9], B. Marangelli[1], W. Menn[9], J.W. Mitchell[5], A. Morselli[8], J.F. Ormes[5], P. Papini[3], A. Perego[3], S. Piccardi[3], P. Picozza[8], M. Ricci[4], P. Schiavon[12], M. Simon[9], R. Sparvoli[8], P. Spillantini[3], P. Spinelli[1], S.A. Stephens[2], S.J. Stochaj[6], R.E. Streitmatter[5], M. Suffert[11], A. Vacchi[12], N. Weber[10], N. Zampa[12]

.

1. Dipartimento di Fisica dell'Università and Sezione INFN di Bari, Via Amendola 173, I-70126 Bari, Italy

2. Tata Institute of Fundamental Research, Homi Bhabha Road, Bombay 400 005, India

3. Dipartimento di Fisica dell'Università and Sezione INFN di Firenze, Largo Enrico Fermi 2, I-50125 Firenze, Italy

4. Laboratori Nazionali INFN, Via Enrico Fermi 40, CP 13, I-00044 Frascati, Italy

5. NASA/Goddard Space Flight Center, Greenbelt, MD 20771, USA

6. New Mexico State University, Las Cruces, NM 88003, USA

7. Dipartimento di Fisica dell'Università and Sezione INFN di Perugia, Via Pascoli, I-06100 Perugia, Italy

8. Dip. di Fisica dell'Università and Sezione INFN di Roma, Tor Vergata, Via della Ricerca Scientifica 1, I-00133 Roma, Italy

9. Universität Siegen, 57068 Siegen, Germany

10. Royal Institute of Technology, Frescativagen 24, S-104 05 Stockholm, Sweden

11. Centre des Recherches Nucléaires, BP20, F-67037 Strasbourg-Cedex, France

12. Dipartimento di Fisica dell'Università and Sezione INFN di Trieste, Via A. Valerio 2, I-34147 Trieste, Italy

Subject headings: Cosmic rays: abundances - elementary particles

.

Prefered to be published as a letter in the main journal

.

Corresponding author:

Tom Francke

Royal Institute of Technology

Frescativagen 24

S-104 05 Stockholm

Sweden

Tel: + 46 8 16 10 00

Telefax: +46 8 15 86 74

E-mail: francke@particle.kth.se

Received _____; accepted _____

ABSTRACT

We report on the positron to electron ratio in the cosmic radiation over more than one decade in energy from 0.85 to 14 GeV, using the NMSU-WiZard/CAPRICE balloon borne magnet spectrometer. The spectrometer uses a solid radiator RICH detector and a silicon-tungsten calorimeter for particle identification. The proton rejection factor of the two instruments combined is better than 2×10^{-6} between 0.6 and 3 GV/c dropping to 6×10^{-5} at 5 GV/c and 10^{-4} at 10 GV/c. The data was collected during 23 hours at a mean residual atmosphere of 4.0 g/cm^2. From a total of 2756 well identified e^- and 498 e^+ we are able to construct the positron fraction $R = e^+ /(e^+ + e^-)$ as a function of energy with small errors from 0.85 GeV to 14 GeV for the first time. We observe a decreasing ratio in this energy region. This energy dependent behaviour is consistent with the simple leaky box model. The positron fraction in the upper energy bins are in agreement with the latest high energy measurements.

1. Introduction

It is generally believed that the bulk of cosmic ray positrons above about 100 MeV are of secondary origin, being produced in high energy collisions of cosmic ray nucleons with interstellar matter (Protheroe 1982). By this process electrons are also produced in approximately equal amounts as positrons. However, most of the cosmic ray electrons, which are only about 1% of the total cosmic ray flux, come from primary production sites. The fraction of positrons $R = e^+ /(e^+ + e^-)$ is a sensitive parameter for understanding production and propagation of the lightest charged lepton. In addition, the solar wind could influence the positrons and electrons differently, making R time dependent over the period of the solar cycle.

Most of the recent measurements on the electron-positron component have been carried out above 5 GeV (e.g. Barwick et al. 1995, Golden et al. 1996). Except for one measurement with rather large uncertainties (Clem et al. 1995), no measurements have been made below 5 GeV since early seventies (Fanselow et al. 1969, Daugherty et al. 1975). The major problems associated with the balloon borne positron measurements are (i) the unique identification against a vast background of protons, and (ii) corrections for the positrons produced in the residual atmosphere.

In this letter we are reporting results from a balloon borne experiment in which the positrons were identified with a negligible background from protons in the energy range between 0.6 and 10 GeV, measured at the spectrometer, by using the combination of a ring imaging cherenkov (RICH) detector and an imaging silicon-tungsten calorimeter. This was the first time that such a powerful combination of detectors was used in cosmic ray studies.

In order to account for the atmospheric corrections, we have made use of a novel technique. This method involves first using the instrument to determine the negative muon spectrum at float altitude. This spectrum is then used to normalize the analytically

determined atmospheric electron-positron spectra. This method is reliable since most of the atmospheric electrons and positrons at small atmospheric depths are produced from muon decay at these energies.

2. Detector system

Figure 1 shows the NMSU-WiZard/CAPRICE spectrometer that was flown from Lynn Lake, Manitoba, Canada on August 8, 1994. From top to bottom it includes a RICH detector, a time-of-flight (ToF) system, a magnet spectrometer of multiwire proportional chambers (MWPC) and drift chambers (DC) and a silicon-tungsten imaging calorimeter.

The RICH detector (Carlson et al. 1994, Carlson et al. 1995), with a threshold Lorentz factor of 1.5, uses a solid NaF radiator and a photosensitive MWPC with pad readout to detect the Cherenkov light image. It was used to measure the velocity of the particles. The ToF system consists of two layers of plastic scintillators, one above and one below the tracking stack. It was used to give a trigger as well as to measure the time-of-flight and dE/dx losses of the particles. The magnet spectrometer (Golden et al. 1991, Hof et al. 1994) measures the rigidity of the particle with an average maximum detectable rigidity of 200 GV/c. Finally, the electromagnetic calorimeter (Bocciolini et al. 1996) is composed of eight planes of double-sided silicon strip detectors interleaved with seven layers of tungsten converters (each one radiation length thick). The silicon strips are placed perpendicular to each other, giving the energy deposited in each strip. Moreover, this imaging device provides information on the longitudinal as well as the lateral profile of the cascade.

3. Data analysis

During the 23 hour long flight more than six million events were recorded at a mean residual atmosphere of 4.0 g/cm^2. Electrons and positrons were selected in the rigidity range between 0.6 and 10 GV/c. We required that a single track with an acceptable chi-square traversed the spectrometer. We selected singly charged particles with a signal corresponding to less than 1.7 mips (minimum ionizing particles) in the top ToF scintillator. Albedo events were rejected using both the ToF and the RICH. An electron sample was selected as particles with negative deflection, $\beta = 1$ as detected by the RICH and an electromagnetic shower in the calorimeter.

The cuts imposed on the calorimeter to identify electromagnetic showers have a logarithmic dependence on rigidity and are based on (a) results from an experiment using particle beams at CERN (Bocciolini et al. 1993), (b) simulations and (c) experience gained from a previous flight with the same instrument (Golden et al. 1996). An electromagnetic shower is characterized by a narrow shower with most of the energy deposited inside 4 Molière radii around the track. We imposed additional cuts based on the total detected energy, which should match the measured momentum, and on the longitudinal and lateral profiles of the shower. A small number of particles emit a bremsstrahlung photon before entering the calorimeter (e.g. in the RICH or the aluminum cover of the gondola) that was detected in the calorimeter as a parallel shower. These double shower events with a single track in the tracking system are clearly electron/positron events and can be used with looser cuts. The detection efficiency of the calorimeter using the above cuts is rigidity dependent increasing from 80% at 0.6 GV/c to 85% above 0.7 GV/c, being constant 85% between 0.7 and 3 GV/c then slowly decreasing to 75% at 10 GV/c.

The RICH was used to measure the velocity (β) of the particles. Due to the high rejection factor of the calorimeter, rather loose cuts were applied on the RICH data in order

to maximize the efficiency of selection. Electrons and positrons were selected by the RICH as $\beta = 1$ particles with a well defined Cherenkov light image and a good agreement between the position determined by the RICH and that from the tracking measurement. With these cuts applied, the RICH has a constant detection efficiency of 72% between 0.6 and 5 GV/c. Above 5 GV/c the RICH is not capable of separating protons from positrons and was not used.

The scintillator cut of $\leq$1.7 mip gave an efficiency of 98% for protons, pions and muons. Electrons and positrons can emit bremsstrahlung photons which materialize in or above the top scintillator. These events will be rejected by the cuts applied. The efficiency for electrons and positrons is found to be decreasing from 86% at 0.6 GeV to 81% at 10 GeV due to a small increase in shower multiplicity.

4. Results

Table 1 gives the number of electrons and positrons that pass the cuts applied on the RICH, the ToF and the calorimeter. In order to estimate the number of protons which simulate a positron-like cascade in the calorimeter, we selected a proton sample using the RICH and ToF for rigidities less than 1.4 GV/c. In this energy region the RICH acts as a threshold counter and the ToF is able to separate protons from lighter particles. Between 1.4 and 5.0 GV/c the RICH can accurately identify protons. On this proton sample the calorimeter cuts were applied and the surviving protons were used to determine the contamination. The proton contamination was found to be 8×10^{-4} for rigidities between 0.6 and 1.0 GV/c and less than 1×10^{-4} between 1 and 5 GV/c. In the energy region from 5 to 10 GV/c we assumed that the contamination is the same as that of the bin 3 to 5 GV/c , that is: $(1.1 \pm 0.5) \times 10^{-4}$.

The muon and pion background was estimated using Monte Carlo simulations. The

pion contamination was found to be 5×10^{-3} below 1 GV/c and less than 1×10^{-3} between 1 and 5 GV/c. However, the abundance of pions is less than 1×10^{-3} of the protons at this small atmospheric depth and hence the pion contamination is insignificant. The muon contamination was negligible at all rigidities.

The number of protons passing the RICH cuts was estimated using a proton sample selected by the ToF below 1 GV/c, and by the calorimeter above 1 GV/c by requiring an hadronic interaction. The proton contamination in the RICH was found to be 2×10^{-3} between 0.6 and 1 GV/c increasing to 2% at 3 GV/c, 30% at 4 GV/c and 60% at 5 GV/c due to the loose cuts applied. It may be pointed out that the RICH cannot separate muons and pions from electrons and positrons in the energy region of interest in this analysis.

Assuming that the rejection of protons by the RICH and the calorimeter is independent we get a total proton contamination of less than 2×10^{-6} between 0.6 and 3 GV/c increasing to 6×10^{-5} at 5 GV/c and 10^{-4} at 10 GV/c. The rejection factor of the calorimeter and the RICH is high enough to eliminate all proton, pion and muon contamination from the positron sample between 0.6 and 3 GV/c. The proton contamination was found to be 9% and 17% of the positron sample in the rigidity bins 3 to 4 GV/c and 4 to 5 GV/c, respectively. In the rigidity region 5 to 10 GV/c only the calorimeter has been used resulting in a proton contamination of 25% of the selected positron sample. This proton contamination is shown in the parenthesis in Table 1 and was subtracted from the positron sample.

The secondary positrons and electrons, which are produced in the residual atmosphere above the instrument were estimated in the following manner. We first determined the energy spectrum of the negative muons. These muons were identified by requiring minimum ionizing, negative curvature particles, which enter the instrument from the top and undergo no interaction in the calorimeter. The efficiency of selecting these particles was found to be

98.2%. We show in Fig. 2 the observed spectrum (number of particles per unit energy) of muons from 0.8 GeV to 15 GeV. The dotted curve shown in this figure is the calculated spectrum at 4 g/cm^2 of residual atmosphere (Stephens 1981). Note the excellent agreement with data. At the top of the payload (ToP) most secondary electrons and positrons come from decaying muons. We use the normalization constant obtained from the muon spectrum in Fig. 2 to estimate the secondary electron-positron spectra at 4 g/cm^2 (Stephens 1981).

The observed electron and positron spectra were corrected for the efficiencies and were extrapolated to the top of the payload using bremsstrahlung corrections. These flux values (particles per unit energy) are shown in Fig. 2 as a function of energy. The estimated atmospheric secondary electrons and positrons are also shown by dashed and solid curves, respectively. The number of secondary particles are tabulated in Table 1 along with the extrapolated number of observed electrons and positrons to the top of the payload.

In order to check the correctness of this procedure, we have constructed the growth curve of the electrons in the atmosphere from 4 g/cm^2 to 200 g/cm^2 in the energy interval 0.6-0.9 GeV. By normalizing the calculated growth curve (Daniel and Stephens 1974) for 700 MeV electrons over the depth between 30 and 150 g/cm^2, we obtained the fraction of secondary electrons to be 13.2$\pm$1.9% at 4 g/cm^2. From the Table 1, one can estimate that the fraction of secondary electrons in the energy interval between 0.6 and 0.8 GeV is 15.1$\pm$2.3%, assuming a possible 15% uncertainty for the theoretical estimate. This observed consistency between these two independent methods gives us confidence that the corrections made are reliable.

The corrected electron and positron spectra were extrapolated to the top of the atmosphere (ToA) by solving simultaneously the cascade equations describing the propagation of electrons, positrons and gamma rays that result from bremsstrahlung of the electron component (Stephens 1981). From this, we obtained the positron to electron ratios

that are shown in Table 1 along with the median energy at the top of the atmosphere.

The resulting positron to electron ratio is plotted in Fig. 3 together with previous measurements (Fanselow et al. 1969, Daugherty et al. 1975, Muller and Tang 1987, Golden et al. 1987, Golden et al. 1994, Barwick et al. 1995, Golden et al. 1996, Agrinier et al. 1969, Clem et al. 1995). The errors shown includes both the statistical and the systematic errors. Our results are in agreement with the recent measurements (Golden et al. 1996, Barwick et al. 1995) at the upper energy bins. We notice that the positron fraction (R) decreases from 0.14 at 0.8 GeV to 0.075 at 4 GeV and remains nearly constant above this energy. The observed energy dependence of our results is consistent with that expected from the simple leaky box model (Protheroe 1982). The value of the ratio is dependent on the amount of matter traversed in the interstellar space and on the assumed spectrum of electrons; both these have large uncertainties. It is essential to obtain the absolute spectra of both electrons and positrons to derive useful information on the origin and propagation of these components. The analysis to obtain absolute fluxes of electrons and positrons is in progress as well as efforts to extend the analysis to lower energies.

This work was supported by NASA Grant NAGW-110, The Istituto Nazionale di Fisica Nucleare, Italy, the Agenzia Spaziale Italiana, DARA and DFG in Germany, EU SCIENCE, the Swedish National Space Board and the Swedish Council for Planning and Coordination of Research. We wish to thank the National Scientific Balloon Facility and the NSBF launch crew that served in Lynn Lake. We would also like to acknowledge the essential support given by the CERN TA-1 group and the technical staff of NMSU and of INFN.

REFERENCES

Agrinier, B. et al. 1969, Lett. Nuovo Cimento, 1, 153

Barwick, S.W. et al. 1995, Phys. Rev. Lett., 75, 390

Bocciolini, M. et al. 1993, Nucl. Instr. and Meth., A333, 77

Bocciolini, M. et al. 1996, Nucl. Instr. and Meth., A370, 403

Carlson, P. et al. 1994, Nucl. Instr. and Meth., A349, 577

Carlson, P. et al. 1995, To appear in Nucl. Instr. and Meth.

Clem, J. et al. 1995, Proc. 24th Int. Cosmic Ray Conf., Rome, Vol. 3, 5

Daniel, R. R. and Stephens, S. A. 1974, Rev. Geoph. and Sp. Ph., Vol.12, 233

Daugherty, J. K. et al. 1975, ApJ, 198, 493

Fanselow, J. L. et al. 1969, ApJ, 158, 771

Golden, R. L. et al. 1987, A&A, 188, 145

Golden, R. L. et al. 1991, Nucl. Instr. and Meth., A306, 366

Golden, R. L. et al. 1994, ApJ, 436, 769

Golden, R. L. et al. 1996, ApJ, 457, 103

Hof, M. et al. 1994, Nucl. Instr. and Meth., A345, 561

Muller, D., & Tang, K. K. 1987, ApJ, 312, 183

Protheroe, R. J. 1982, ApJ, 254, 391

Stephens, S. A. 1981, Proc. 17th Int. Cosmic Ray Conf., Paris, Vol.4, 282, Vol.2, 512

Fig. 1.— Schematic diagram of the CAPRICE apparatus.

Fig. 2.— The measured electron and positron flux at the top of the payload and the analytically determined atmospheric background, together with the measured muon spectrum and the analytical prediction.

Fig. 3.— Positron fraction $e^+ / (e^+ + e^-)$ as observed in this experiment compared with other published data and a simple leaky box model.

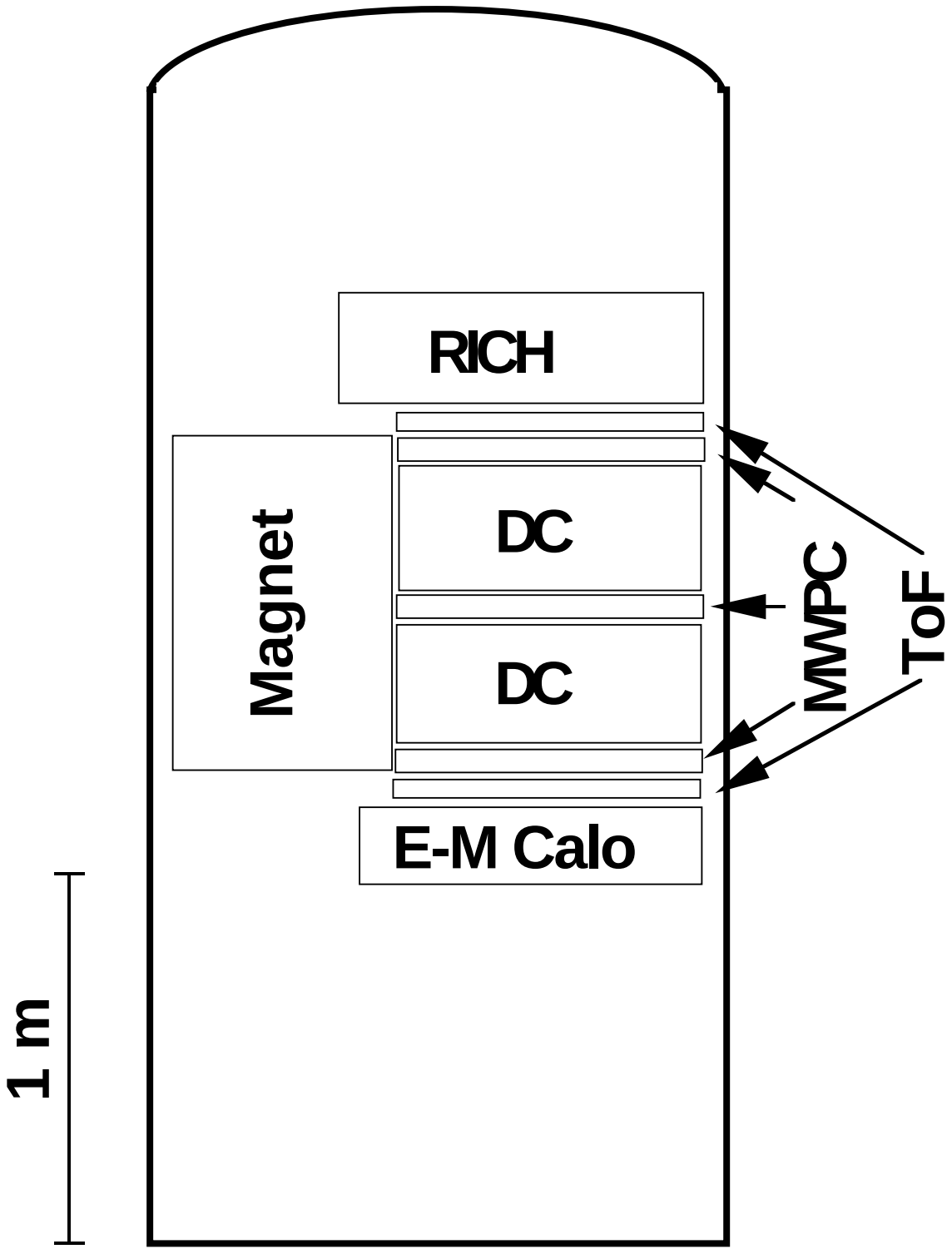
RICH
DC
DC
Magnet
MWPC
ToF
E-M Calo
1 m

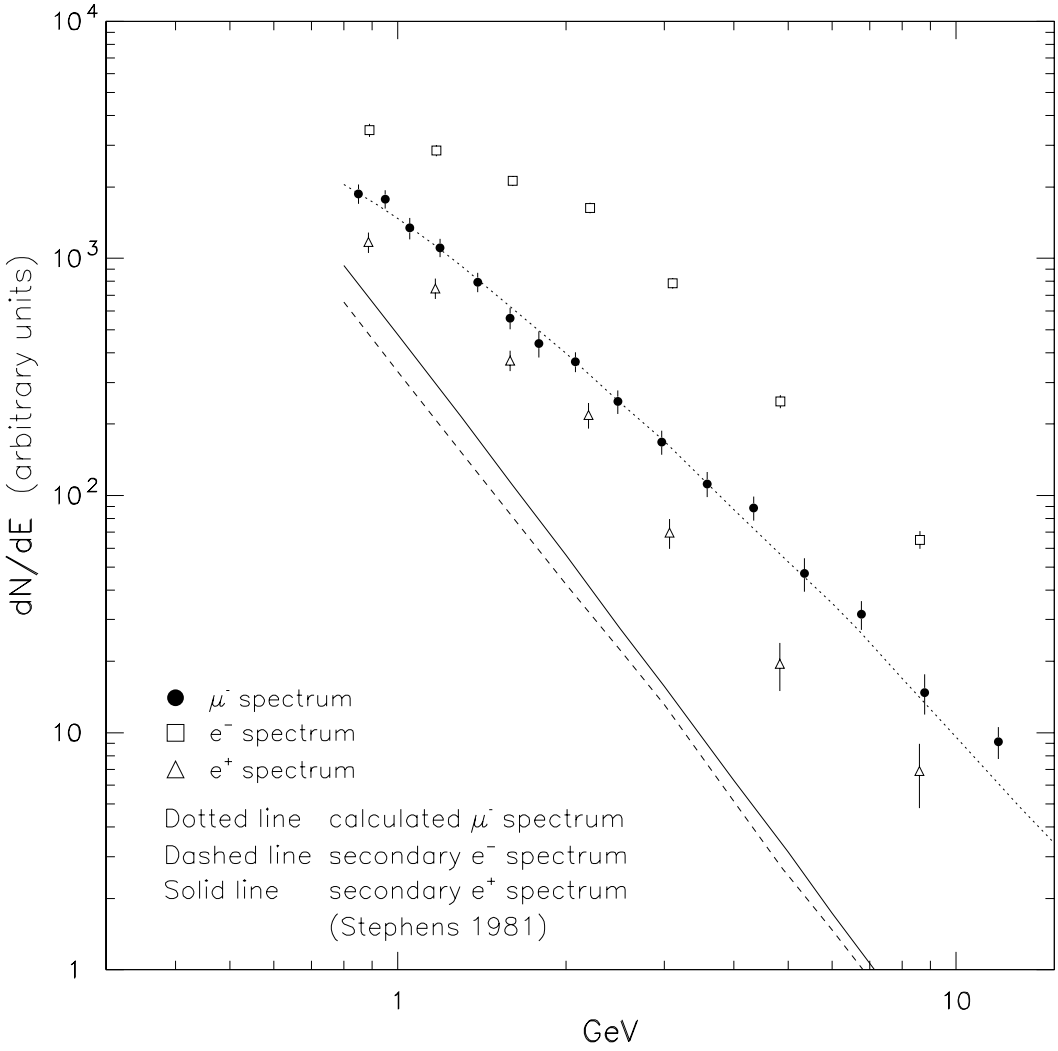
10^4
10^3
10^2
10
1
dN/dE (arbitrary units)
1
10
GeV
μ^- spectrum
e^- spectrum
e^+ spectrum
Dotted line calculated μ^- spectrum
Dashed line secondary e^- spectrum
Solid line secondary e^+ spectrum
(Stephens 1981)

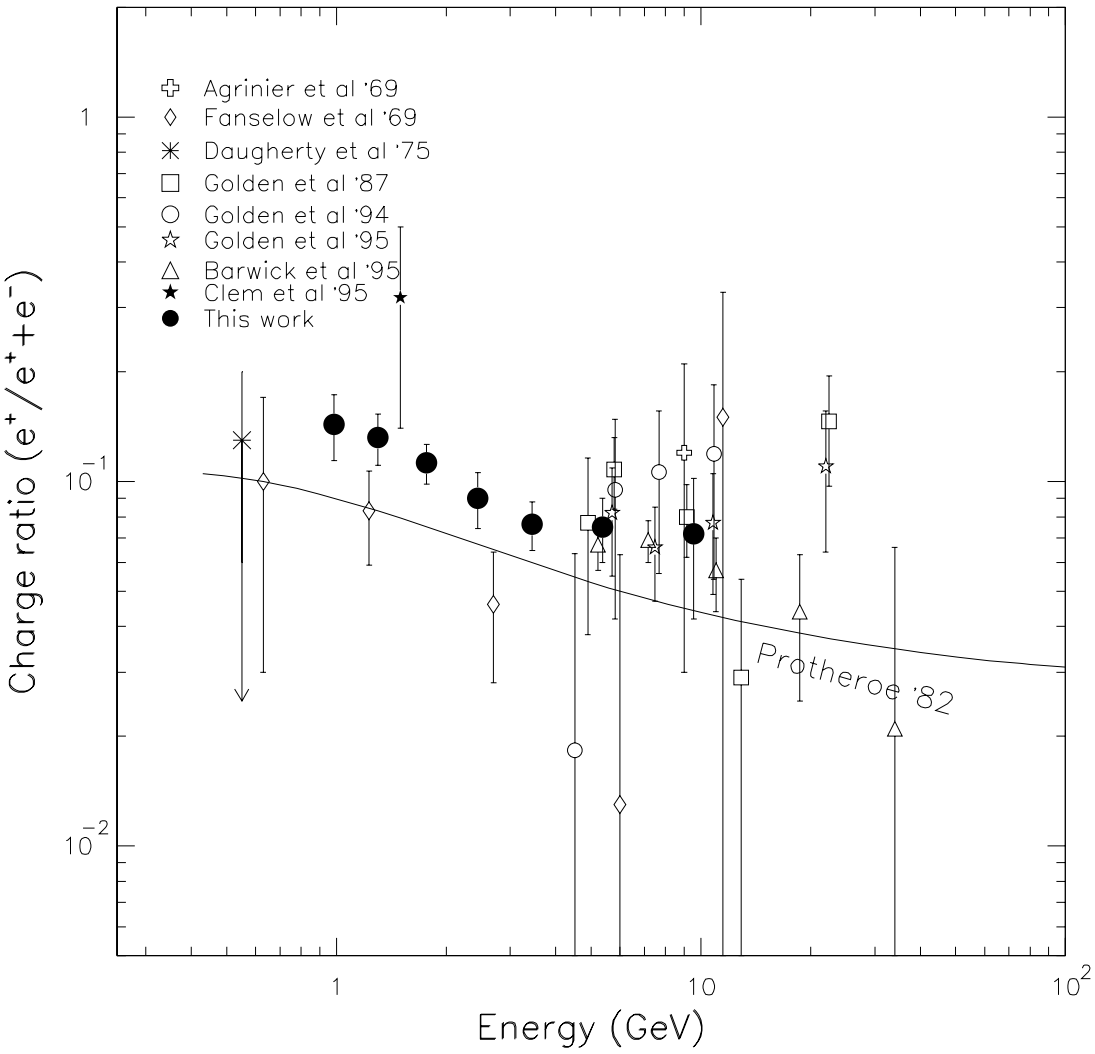
Agrinier et al '69
Fanselow et al '69
Daugherty et al '75
Golden et al '87
Golden et al '94
Golden et al '95
Barwick et al '95
Clem et al '95
This work
Protheroe '82
Charge ratio ($e^+/e^+ + e^-$)
Energy (GeV)
1
10^{-1}
10^{-2}
1
10
10^2

Table 1. Summary of electron - positron results.

Energy bin at spectrometer GeV	Observed number of events[a]		Extrapolated number at ToP[b]		Atmospheric correction		Median energy at ToA[c]	$\frac{e^+}{e^+ + e^-}$ at ToA[c]
	e^-	e^+	e^-	e^+	e^-	e^+	GeV	
0.6 - 0.8	396	121	886.4	300.4	125.5	184.8	0.99	0.14 ± 0.03
0.8 - 1.05	415	105	905.7	237.6	67.6	94.6	1.30	0.132 ± 0.021
1.05 - 1.5	554	103	1212.6	212.4	45.9	65.9	1.77	0.113 ± 0.014
1.5 - 2.0	447	65	1040.2	139.2	20	26.6	2.45	0.090 ± 0.016
2.0 - 3.0	455	49	1003.4	88.9	14.8	18.1	3.45	0.076 ± 0.012
3.0 - 5.0	303	28(4)	632.5	49.4	7	8.6	5.37	0.075 ± 0.015
5.0 - 10.0	186	27(7)	414.8	43.9	2.9	3.4	9.56	0.07 ± 0.03

[a]The numbers shown in the brackets are the estimated proton background.

[b]Top of the payload.

[c]Top of the atmosphere.